

Learning with Alignments: Tackling the Inter- and Intra-domain Shifts for Cross-multidomain Facial Expression Recognition

Yuxiang Yang[†]

yangyuxiang3@stu.scu.edu.cn
Sichuan University
Chengdu, Sichuan

Yuanyuan Xu

YuanyuanXuSCU@outlook.com
Sichuan University
Chengdu, Sichuan

Lu Wen[†]

wenlu0416@stu.scu.edu.cn
Sichuan University
Chengdu, Sichuan

Xi Wu

wuxi@cuit.edu.cn
Chengdu University of Information
Technology
Chengdu, Sichuan

Yan Wang*

wangyanscu@hotmail.com
Sichuan University
Chengdu, Sichuan

Xinyi Zeng

percyzy@qq.com
Sichuan University
Chengdu, Sichuan

Jiliu Zhou

zhoujiliu@cuit.edu.cn
Sichuan University
Chengdu, Sichuan

ABSTRACT

Facial Expression Recognition (FER) holds significant importance in human-computer interactions. Existing cross-domain FER methods often transfer knowledge solely from a single labeled source domain to an unlabeled target domain, neglecting the comprehensive information across multiple sources. Nevertheless, cross-multidomain FER (CMFER) is very challenging for (i) the inherent inter-domain shifts across multiple domains and (ii) the intra-domain shifts stemming from the ambiguous expressions and low inter-class distinctions. In this paper, we propose a novel Learning with Alignments CMFER framework, named LA-CMFER, to handle both inter- and intra-domain shifts. Specifically, LA-CMFER is constructed with a global branch and a local branch to extract features from the full images and local subtle expressions, respectively. Based on this, LA-CMFER presents a dual-level inter-domain alignment method to force the model to prioritize hard-to-align samples in knowledge transfer at a sample level while gradually generating a well-clustered feature space with the guidance of class attributes at a cluster level, thus narrowing the inter-domain shifts. To address the intra-domain shifts, LA-CMFER introduces a multi-view intra-domain alignment method with a multi-view clustering consistency constraint where a prediction similarity matrix is built to pursue consistency between the global and local views, thus refining pseudo labels and eliminating latent noise. Extensive experiments on six benchmark datasets have validated the superiority of our LA-CMFER.

CCS CONCEPTS

• Computing methodologies → Artificial intelligence; • Human-centered computing → Human computer interaction (HCI)

KEYWORDS

Cross-multidomain adaptation, Inter- and intra-domain shifts, Facial expression recognition, Domain alignments

1 Introduction

Facial Expression Recognition (FER) endeavors to discern human expressions and emotional states, playing a pivotal role in human-computer interactions [1]. Nowadays, FER has gained notable promotion thanks to diverse deep learning (DL) algorithms [2, 3, 4, 5, 46, 47, 48] and well-annotated FER datasets [6, 7, 8]. However, these FER works [9, 10] typically operate under the assumption that both training and testing samples come from the same dataset (domain) and inherently share an identical data distribution. In practice, their classification accuracy often drops sharply due to the great discrepancy in data distribution (i.e., inter-domain shifts) [11, 12] when applied in different scenes, making them incapable of tackling the cross-domain problem settings.

To alleviate the inter-domain shifts, unsupervised Cross-Domain FER (CDFER) [13, 14, 49] has been introduced, aiming to extract domain-invariant features from a single labeled source domain to accurately classify the samples in an unlabeled target domain. Various techniques, such as adversarial learning [11, 15, 16] and metric learning [12, 17, 18], have been explored to reduce the distribution disparity between the two domains. However, these methods primarily focus on leveraging data information from a single source, while overlooking the valuable facial knowledge buried in multiple source domains. In reality, there are multiple labeled source datasets collected with diverse conditions, such as different acquisition environments, ethnic characteristics, etc. Leveraging these sources can significantly increase the number of training samples and further provide more comprehensive and

* Corresponding author

[†] The two authors contribute equally to this work.

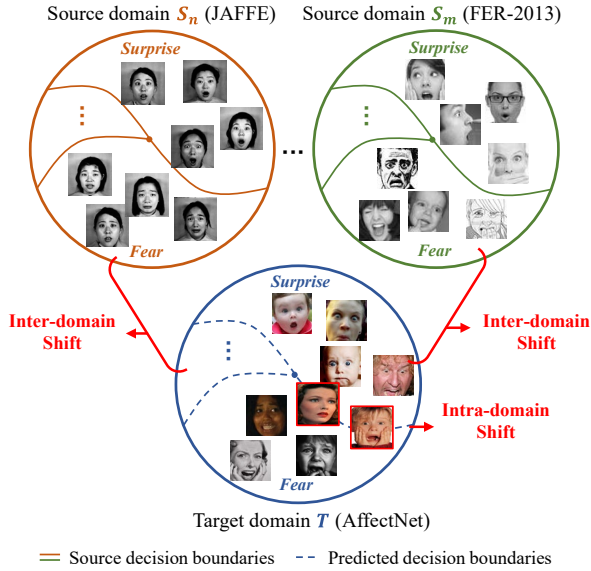


Fig. 1. Illustration to the problem setting of CMFER task where both inter-domain shifts (different data distributions) and intra-domain shifts (ambiguous expressions and low inter-class distinctions near the target decision boundaries) exist.

discriminative feature representations of facial expressions, thus contributing to better generalization ability. Subsequently, unsupervised Cross-Multidomain FER (CMFER) [19] is motivated to effectively transfer richer facial knowledge from multiple labeled source domains to the unlabeled target domain.

A simple solution to CMFER tasks is to regard different sources as a single source and directly apply CDFER methods. Regrettably, as the number of sources increases, these approaches often exhibit sub-optimal performance or even degradation owing to the growing complexity of data distributions [19, 20]. Therefore, developing a well-designed CMFER method is quite imperative. Delving deeply into CMFER, there are two main challenges. The first one is the above-mentioned *inter-domain shifts across different domains* due to their inherent data distribution difference. Specifically, as shown in Fig.1, with different shooting conditions, AffectNet [6] (i.e., T) contains both gray and color images, while FER-2013 [21] (i.e., S_m) only includes gray images. Besides, JAFFE [22] (i.e., S_n) has notable racial characteristics where all the facial images come from Japanese women. These severe inter-domain shifts disrupt the effective extraction of domain-invariant facial expression representations and hinder smooth knowledge transfer from source domains to the target domain. The second challenge for CMFER is the *intra-domain shifts that occur within the target domain*. As shown in Fig.1, the subtle differences and intrinsic ambiguities in human expressions (marked by red borders) may lead to lower inter-class distinctions. Therefore, the intra-domain shifts are likely to cause the model to produce uncertain category predictions and acquire inaccurate semantic information, severely damaging the prediction robustness.

In this paper, we propose a novel Learning with Alignments for Cross-Multidomain Facial Expression Recognition (LA-CMFER)

framework to simultaneously tackle the inter- and intra-domain shifts. In LA-CMFER, we consider both essential global and local features for facial expressions and employ a shared dual-branch structure across multiple source domains and the target domain. Then, to address the inter-domain shifts, a dual-level (i.e., sample-level and cluster-level) inter-domain alignment is developed to encourage the model to pay more attention to the hard-to-align samples with higher uncertainty and generate a more well-clustered feature space based on the predicted labels. As for the intra-domain shifts, a multi-view intra-domain alignment is devised with a multi-view clustering consistency constraint to form a discriminative target feature space, and a multi-view voting scheme to gain the high-quality pseudo labels for an effective information interaction between the local and global branches, respectively. Both inter- and intra-domain alignments act with united strength to comprehensively extract discriminative facial representations from multiple source domains and promote the classification in the target domain. The main contributions of this paper are three-fold:

- We present a Learning with Alignments for Cross-Multidomain Facial Expression Recognition (LA-CMFER) framework to tackle both inter- and intra-domain shifts and utilize beneficial knowledge from multiple source domains to address the challenging CMFER task.
- To mitigate the inter-domain shift, we introduce a dual-level inter-domain alignment method that prioritizes hard-to-align samples and fosters a well-clustered feature space. As for the intra-domain shift, we design a multi-view clustering consistency constraint between the global and local branches to gain a concentrated target feature space for alleviating the interference of noisy samples.
- Extensive experiments on six commonly used FER benchmark datasets verify the superior performance of our method compared to other state-of-the-art approaches.

2 Related Works

2.1 Cross-domain FER

CDFER follows the fundamental principles of Unsupervised Domain Adaptation (UDA) [23], aiming to apply the classifier trained with a single labeled source domain to classify samples in an unlabeled target domain. Numerous studies have focused on CDFER tasks, which can be categorized into two groups: metric-based approaches vs. adversarial-based approaches. Concretely, metric-based approaches [12, 13, 17, 18, 24] construct proper distance functions to extract more discriminative facial features for reducing cross-domain distribution variation. For instance, Ni et al. [24] combined metric learning with dictionary learning to alleviate the transfer facial expression recognition issue. Zhang et al. [13] presented a local-global discriminative subspace transfer learning (LGDSTL) method where a local-global graph is used as distance metric. Besides, adversarial-based approaches [11, 15, 16, 25] mine the domain-invariant facial features with adversarial training. To illustrate, Xie et al. [15] embedded a graph representation propagation with adversarial learning and presented an adversarial

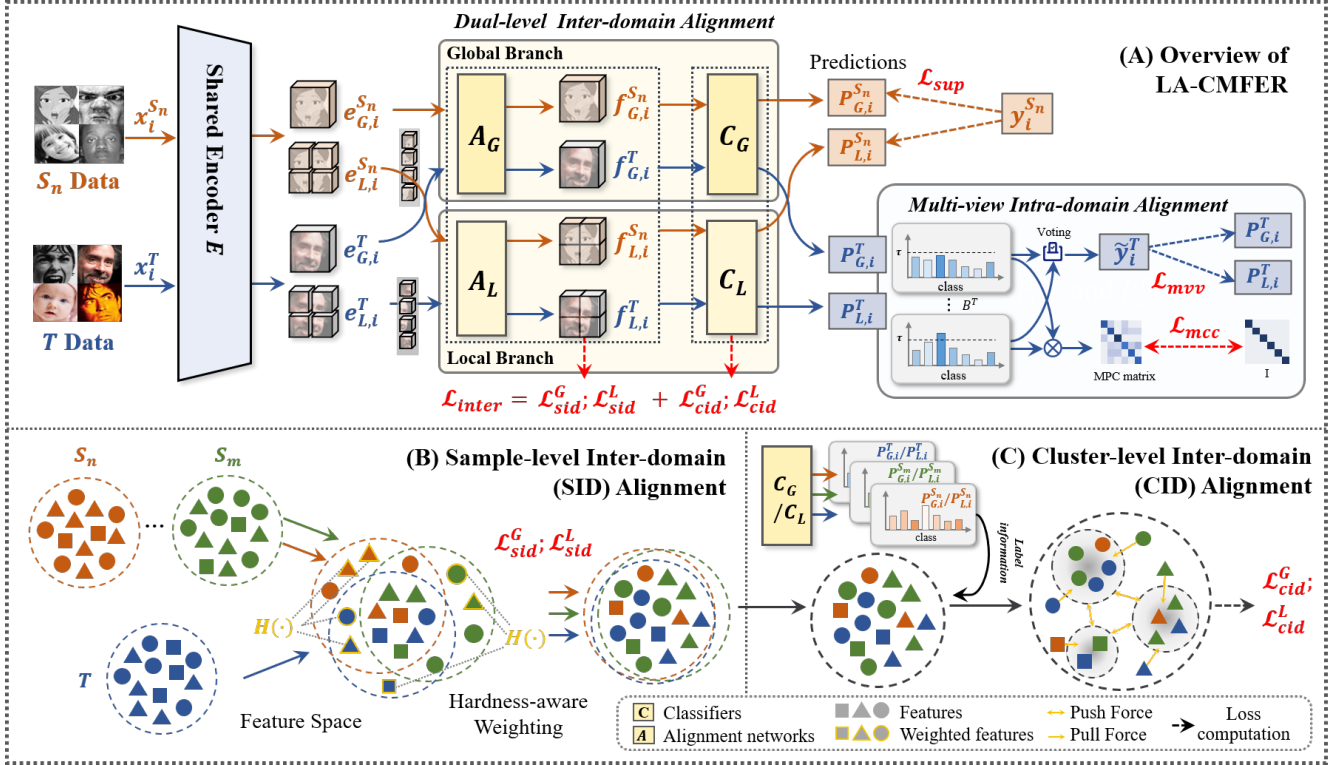


Fig. 2. Overview of our proposed LA-CDFER framework with a dual-level inter-domain alignment and a multi-view intra-domain alignment. Our framework receives samples with labels from $|S_n|$ sources and tries to classify the target samples in \mathcal{D}^T .

graph representation adaptation framework. Considering the important local facial features, Ji et al. [11] proposed a region attention-enhanced CDFER approach to emphasize the local features for minimizing domain discrepancies. Despite their promising results, these methods deal with only one single source and are not competitive in addressing the complex data distributions encountered in cross-multidomain scenarios.

2.2 Multi-source Domain Adaptation

Multi-source Domain Adaptation (MDA) [26] holds the assumption that data can be gathered from diverse source domains with different distributions, which is a more practical but challenging task compared to single-source domain adaptation. Pioneer studies [27, 28, 50] have theoretically confirmed that the target distribution can be represented as a weighted combination of source distributions. To further ensure effective adaptation, the key lies in overcoming the inter-domain shifts caused by diverse data distributions across domains. Along with this philosophy, Zhao et al. [29] used adversarial training to align the target and source distributions. Zhu et al. [30] developed an MDA framework with multiple domain-specific classifiers to mine the domain-invariant features and use a maximum mean discrepancy (MMD) loss [31] to ease the inter-domain shift. Li et al. [32] devised a feature filtration network to selectively align features across domains.

Unlike existing MDA works in natural image classification, the CMFER tasks are more difficult. Besides the inter-domain shifts, the subtle differences between facial expressions also bring about

intra-domain shifts, e.g., low inter-class distinctions in the decision boundaries. In the emerging CMFER, only Liu et al. [19] proposed a domain-uncertain mutual learning (DUML) network based on adversarial learning to consider both inter-domain and intra-domain uncertainty. In this paper, we present the Learning with Alignments framework with dual-level inter-domain alignment and multi-view intra-domain alignment to adeptly address two kinds of domain shifts with a simpler and lighter architecture.

3 Methodology

3.1 Preliminaries and Framework Overview

In the problem definition of CMFER, there are N labeled source domains $\{S_n\}_{n=1}^N$ and an unlabeled target domain T , with a total of K shared facial expression classes. Concretely, S_n denotes the n -th FER dataset $\mathcal{D}^{S_n} = \{(x_i^{S_n}, y_i^{S_n})\}_{i=1}^{|S_n|}$ where $x_i^{S_n}$ is the i -th labeled source image and $y_i^{S_n} \in \{0,1\}^K$ represents its one-hot real label. Correspondingly, the target domain T contains a single unlabeled dataset $\mathcal{D}^T = \{x_i^T\}_{i=1}^{|T|}$, where x_i^T denotes the i -th unlabeled target image. CMFER tries to train a deep model with \mathcal{D}^T and $\{\mathcal{D}^{S_n}\}_{n=1}^N$ to accurately predict the expression labels of x^T in \mathcal{D}^T .

The overview of our LA-CDFER framework is illustrated in Fig. 2, which includes a shared encoder E with both global and local branches. Specifically, the global/local branch is equipped with respective global/local feature alignment network A_G/A_L and feature classifier C_G/C_L . Notably, A_G and A_L hold different model

architectures to respectively mine the expression knowledge from global and local views. In the training stage, the shared encoder E first encodes the source image $x_i^{s_n}$ from the n -th source batch (B^{s_n}) into compact embedding $e_{G,i}^{s_n}$. For the global branch, $e_{G,i}^{s_n}$ is fed into A_G to produce the global feature $f_{G,i}^{s_n}$ and C_G is then utilized to form the final prediction $P_{G,i}^{s_n}$. Meanwhile, we produce a local embedding $e_{L,i}^{s_n}$ by cropping and concatenating $e_{G,i}^{s_n}$ in a grid manner. After the processing of A_L and C_L , the local feature $f_{L,i}^{s_n}$ and prediction $P_{L,i}^{s_n}$ are obtained. The same process is applied to the target image x_i^T , yielding its global/local feature $f_{G,i}^T/f_{L,i}^T$ as well as prediction $P_{G,i}^T/P_{L,i}^T$. To deal with the inter-domain shifts, LA-CMFER uses a dual-level inter-domain alignment with loss \mathcal{L}_{inter} to separately align global and local source domain features with the target ones at both sample- and cluster-levels. For the intra-domain shifts, given $P_{G,i}^T$ and $P_{L,i}^T$, a multi-view consistency constraint loss \mathcal{L}_{mcc} is utilized to ensure consistency between the global and local views while eliminating latent noise. Besides, a multi-view voting scheme is devised after the \mathcal{L}_{mcc} to generate high-quality pseudo labels \hat{y}_i^T and supervise the predictions of the two branches in turn, facilitating the knowledge interaction of the two branches.

3.2 Global and Local Branches

Given the notable importance of both global and local features, LA-CMFER adopts a dual-branch architecture. As shown in Fig. 2, fed with the source image $x_i^{s_n}$, encoder E first obtains its compact embedding $e_{G,i}^{s_n}$, which is then processed into a global feature $f_{G,i}^{s_n}$ using the alignment network A_G . To capture finer details essential for recognizing subtle differences in full-face images, $e_{G,i}^{s_n}$ is further subdivided into four attentional regions: top-left ($e_{tl,i}^{s_n}$), top-right ($e_{tr,i}^{s_n}$), bottom-left ($e_{bl,i}^{s_n}$), and bottom-right ($e_{br,i}^{s_n}$). These embeddings $e_{L,i}^{s_n} = \{e_{tl,i}^{s_n}, e_{tr,i}^{s_n}, e_{bl,i}^{s_n}, e_{br,i}^{s_n}\}$ separately undergo processing by A_L and are then concatenated to form a local feature $f_{L,i}^{s_n}$. Finally, the classifiers C_G and C_L generate predictions $P_{G,i}^{s_n} = C_G(f_{G,i}^{s_n})$ and $P_{L,i}^{s_n} = C_L(f_{L,i}^{s_n})$. Similarly, when processing the target image x_i^T , the same procedure is followed, resulting in two predictions from the two branches, i.e., $P_{G,i}^T = C_G(A_G(E(x_i^T)))$ and $P_{L,i}^T = C_L(A_L(E(x_i^T)))$. These two branches make predictions from the complementary global-local views for both source and target samples, thus better detecting the beneficial expression knowledge.

3.3 Dual-level Inter-domain Alignment

To tackle the inter-domain shifts between source and target distributions, LA-CMFER presents the dual-level (sample- and cluster-level) inter-domain alignment to comprehensively extract the domain-invariant facial features. This is gained by prioritizing hard-to-align samples with higher uncertainty and grouping samples based on their category information.

Sample-level Inter-Domain Alignment. Existing CDFER works usually use the discrepancy-based constraints (e.g., MMD [30, 31, 52], triplet loss [4], and adversarial loss [11, 25]) to minimize the inter-domain shift. Concretely, given the source distribution

$\mathcal{P}^{s_n}(x, y)$ and target distribution $\mathcal{P}^T(x, y)$, the traditional MMD loss [31] can be formulated as follows:

$$\mathcal{L}_{MMD}(\mathcal{P}^{s_n}, \mathcal{P}^T) = \widehat{D}_\kappa(\mathcal{P}^{s_n}, \mathcal{P}^T) = \|\bar{\phi}^{s_n} - \bar{\phi}^T\|_\kappa^2, \quad (1)$$

$$\bar{\phi}^a = \frac{1}{|B^a|} \sum_{i=1}^{|B^a|} \phi_i^a, \quad (2)$$

where ϕ_i^a denotes the average feature mappings of input samples within the batch B^a to the reproducing Kernel Hilbert Space κ and a represents the target domain (T) or the n -th source (S_n).

Despite its satisfactory performance, traditional MMD usually averages the distances among samples with uniform weights, thus neglecting the varying importance of different samples in the alignment. In the CMFER task, some hard-to-align samples, exhibiting higher uncertainty and located near decision boundaries, may offer greater insights into the domain alignment and knowledge transfer, thus warranting increased attention. Thus, we propose the sample-level inter-domain (SID) alignment with a hardness-aware weighting function. Specifically, given an image x_i^a and its prediction $P_{M,i}^a$ with J probability values $\{P_{M,i}^{a,j}\}_{j=1}^J$, where $M = G$ or L denotes different branches and J denotes the number of classes, we use a measurement term $\Omega_M(\cdot)$ to adaptively evaluate the instantaneous hardness of x_i^a in the current iteration:

$$\Omega_M(x_i^a) = \sqrt{\sum_{j=1}^J \mathbb{1}[P_{M,i}^{a,j} \neq \text{Max}(P_{M,i}^a) \text{ or } j \neq \text{rce}](P_{M,i}^{a,j})^2}, \quad (3)$$

where $\mathbb{1}[\cdot]$ is a binary indicator and $\text{Max}(\cdot)$ represents the maximum function. From both local and global views, $\Omega_M(\cdot)$ aims to exclude the maximum probability in x_i^T or set the real class element (rce) to 0 in $x_i^{s_n}$ and then evaluate the L_2 -norm of the remaining elements. This prioritizes uncertain target sample x_i^T or source sample $x_i^{s_n}$ by assigning them with higher weights. Subsequently, $\Omega_M(x_i^a)$ is normalized in B^a to determine the relative weights $H_M(x_i^a)$ to facilitate batch-wise optimization:

$$H_M(x_i^a) = \frac{\Omega_M(x_i^a)}{\sum_{x_k^a \in B^a} \Omega_M(x_k^a)}. \quad (4)$$

Finally, $H_M(\cdot)$ is utilized to modify the traditional MMD loss as our sample-level inter-domain alignment loss \mathcal{L}_{sid}^M :

$$\mathcal{L}_{sid}^M(\mathcal{P}^{s_n}, \mathcal{P}^T) = \|\bar{\phi}_H^{s_n} - \bar{\phi}_H^T\|_\kappa^2, \quad (5)$$

$$\bar{\phi}_H^a = \frac{1}{|B^a|} \sum_{i=1}^{|B^a|} H_M(x_i^a) \cdot \phi_i^a. \quad (6)$$

Notably, $H_M(\cdot)$ can be seamlessly integrated into other discrepancy-based constraints in a plug-and-play way for providing useful perceptions about sample importance.

Cluster-level Inter-domain Alignment. Existing discrepancy-based inter-domain alignments [30, 31] may blindly align samples with different classes closer, potentially impeding the model from learning discriminative features. Thus, we introduce a cluster-level inter-domain alignment to better group samples based on their categories. We use the real label $y_i^{s_n}=k$ and pseudo label $\hat{y}_i^T=\hat{d}$ to denote the category attributes of the source sample $x_i^{s_n}$ and target sample x_i^T , respectively. Then, we minimize the distances between source-target samples of the same category ($\hat{d} = k$) and maximize them for samples of different categories ($\hat{d} \neq k$). This process is summarized as a cluster-level inter-domain alignment loss \mathcal{L}_{cid} :

$$\mathcal{L}_{cid}^M(\mathcal{P}^{s_n}, \mathcal{P}^T) = \left\| \bar{\phi}_{H,k}^{s_n} - \bar{\phi}_{H,\hat{a}=k}^T \right\|_x^2 - \left\| \bar{\phi}_{H,k}^{s_n} - \bar{\phi}_{H,\hat{a} \neq k}^T \right\|_x^2, \quad (7)$$

$$\bar{\phi}_{H,k}^{s_n} = \frac{1}{|B_k^{s_n}|} \sum_{i=1}^{|B_k^{s_n}|} \bar{\phi}_{H,i}^{s_n}, \quad \bar{\phi}_{H,\hat{a}}^T = \frac{1}{|B_{\hat{a}}^T|} \sum_{i=1}^{|B_{\hat{a}}^T|} \bar{\phi}_{H,i}^T, \quad (8)$$

where the hardness-aware function $H(\cdot)$ is retained to dynamically balance the importance of each sample. As \mathcal{L}_{cid} optimizes, we can achieve a more fine-grained alignment to foster an intra-class convergence while promoting inter-class divergence.

Finally, the dual-level inter-domain alignment is performed in both global and local branches at the same time, thus deriving the following inter-domain loss \mathcal{L}_{inter} :

$$\mathcal{L}_{inter}(\mathcal{P}^{s_n}, \mathcal{P}^T) = \sum_{n=1}^N [(\mathcal{L}_{sid}^G + \mathcal{L}_{sid}^L) + \lambda(\mathcal{L}_{cid}^G + \mathcal{L}_{cid}^L)], \quad (9)$$

where λ is a hyper-parameter for balancing these two terms. Notably, for all domains, we include only those samples whose maximum prediction probability exceeds a predefined reliability threshold ϵ , thus preventing unreliable knowledge transfer from excessively uncertain samples.

3.4 Multi-view Intra-domain Alignment

Multi-view Clustering Consistency Constraint: The intra-domain shifts within the FER target domain are typically characterized by noisy samples near the decision boundary, which may lead to a dispersed target feature space, thereby introducing prediction bias. To tackle this, we propose a novel multi-view clustering consistency constraint, aiming to shape a discriminative and concentrated target feature space. In this space, clusters with the same class predicted by classifiers of different branches should remain similar, while those of different classes should be distinct. Specifically, given the predictions $P_{G,B}^T$ and $P_{L,B}^T$ of all target samples in the target batch B^T from the global and local branches, we build a Multi-view Prediction Consistency (MPC) matrix to evaluate the consistency between these predictions with the following formulation:

$$MPC = (P_{G,B}^T)' \otimes P_{L,B}^T. \quad (10)$$

Drawing on the cluster assumption [33], we consider target samples in B^T as a specific class (i.e., class c) and their corresponding prediction probabilities in B^T as a batch-wise cluster representation for class c , which is captured by the c -th column in $P_{G,B}^T$ or $P_{L,B}^T$. To reach the intra-domain alignment, we enhance the consistency among cluster representations for identical class assignments (i.e., higher diagonal values in MPC) and inconsistency among them with different class assignments (i.e., lower off-diagonal values in MPC). This process can be represented as the following multi-view clustering consistency loss \mathcal{L}_{mcc} :

$$\mathcal{L}_{mcc} = \frac{1}{2c} (S(\|MPC\| - I) + S(\|MPC'\| - I)), \quad (11)$$

where $S(\cdot)$ calculates the sum of absolute values across all matrix elements, $I \in \mathbb{R}^{K \times K}$ represents an identity matrix, and $\|\cdot\|$ denotes a normalization function [34]. Minimizing \mathcal{L}_{mcc} facilitates the well-separated clusters of different expressions in the target feature space and encourages consistent predictions from dual branches.

Multi-view Voting Scheme: Considering the high-quality pseudo labels can provide more accurate guidance, we propose a multi-view scheme with two voting conditions to select them: (i) global

and local branch makes consistent predictions from different views, i.e., $\text{argmax}(P_{G,i}^T) = \text{argmax}(P_{L,i}^T)$; (ii) at least one branch achieves higher confidence than a threshold τ , i.e., $\text{Max}(P_{G,i}^T) > \tau$ or $\text{Max}(P_{L,i}^T) > \tau$. When the two points are all satisfied, the high-quality pseudo-label \tilde{y}_i^T is selected. Additional supervision is then provided to $P_{G,i}^T$ and $P_{L,i}^T$ using a multi-view voting loss \mathcal{L}_{mvv} :

$$\mathcal{L}_{mvv} = \frac{1}{|B^T|} \sum_{i=1}^{|B^T|} \mathbb{1}[MV(P_{G,i}^T, P_{L,i}^T)] \times [CE(P_{G,i}^T, \tilde{y}_i^T) + CE(P_{L,i}^T, \tilde{y}_i^T)], \quad (12)$$

where $MV(\cdot)$ is a function to determine whether the two voting conditions are simultaneously met. By incorporating \mathcal{L}_{mcc} and \mathcal{L}_{mvv} , LA-CMFER is guided to achieve a meaningful knowledge interaction between the two branches, promoting mutual enhancement and facilitating the development of a more robust target feature space.

3.5 Training Objective

The whole training objective contains five parts: (1) supervised loss \mathcal{L}_{sup} for labeled source samples, (2) inter-domain loss \mathcal{L}_{inter} , (3) multi-view clustering consistency loss \mathcal{L}_{mcc} , and (4) multi-view voting loss \mathcal{L}_{mvv} for unlabeled target samples.

The supervised loss \mathcal{L}_{sup} can be represented as follows:

$$\mathcal{L}_{sup} = \frac{1}{N} \sum_{n=1}^N [CE(P_{L,i}^{s_n}, y_i^{s_n}) + CE(P_{G,i}^{s_n}, y_i^{s_n})], \quad (13)$$

where $CE(\cdot)$ denotes the cross-entropy loss.

Finally, the training objective of LA-CMFER is formulated as:

$$\mathcal{L}_{total} = \mathcal{L}_{sup} + \alpha \mathcal{L}_{inter} + \beta \mathcal{L}_{mcc} + \gamma \mathcal{L}_{mvv}, \quad (14)$$

where α , β , and γ are three weighted hyper-parameters.

The training stage of LA-CMFER is summarized in Algorithm 1. In the inference stage, we take the prediction with a higher probability from the two branches as the final result [51].

Algorithm 1: Training procedure of our LA-CMFER.

- 1: **Input:** $|S_n|$ source datasets $\mathcal{D}^{s_n} = \{(x_i^{s_n}, y_i^{s_n})\}_{i=1}^{|S_n|}$ with their corresponding expression labels and the single target dataset $\mathcal{D}^T = \{x_i^T\}_{i=1}^{|T|}$ without labels.
 - 2: **Initialize:** Initialize the network parameters: θ_E for E , θ_{AG} for A_G , θ_{AL} for A_L , θ_{CG} for C_G , θ_{CL} for C_L .
 - 3: **for** $j = 0$ to $iter_total$ **do**
 - 5: Take out a batch of samples B^{s_n} and B^T from $(x_i^{s_n}, y_i^{s_n})$ and \mathcal{D}^T
 - 6: Compute $P_{G,i}^{s_n} = C_G(A_G(E(x_i^{s_n})))$, $P_{L,i}^{s_n} = C_L(A_L(E(x_i^{s_n})))$, $P_{G,i}^T = C_G(A_G(E(x_i^T)))$, and $P_{L,i}^T = C_L(A_L(E(x_i^T)))$
 - 7: Compute the relative hardness weights $H_M(x_i^T)$ where $M = G$ or L , $a = S_n$ or T with Eq. (4)
 - 8: Compute the sample-level inter-domain alignment loss \mathcal{L}_{sid}^M where $M = G$ or L with Eq. (5)
 - 9: Compute the cluster-level inter-domain alignment loss \mathcal{L}_{cid}^M where $M = G$ or L with Eq. (7)
 - 10: Compute the total inter-domain loss \mathcal{L}_{inter} with Eq. (9)
 - 11: Compute the multi-view clustering consistency loss \mathcal{L}_{mcc} with Eq. (11)
 - 12: **if** $\mathbb{1}[MV(P_{G,i}^T, P_{L,i}^T)]$
 - 13: Compute \tilde{y}_i^T and multi-view voting loss \mathcal{L}_{mvv} with Eq. (12)
 - 14: Compute the supervised loss \mathcal{L}_{sup} with Eq. (13)
 - 15: Update $\{\theta_E, \theta_{AG}, \theta_{AL}, \theta_{CG}, \theta_{CL}\}$ by minimizing Eq. (14)
 - 16: **end for**
-

Table 1: Comparisons (%) with SOTAs across multidomain FER datasets.

Protocols	Methods	Venues	→JAFFE	→RAF-DB	→CK+	→Oulu	→AffectNet	→FER-2013	Avg
Single Best	Source-Only	-	59.15	58.74	77.58	54.21	49.31	51.46	55.67
	LGDSL [13]	TAC 2022	-	45.13	66.67	-	-	33.88	-
	RANDA [11]	TKDE 2021	-	62.48	88.71	-	52.34	-	-
	DMSRL [43]	TMM 2022	68.54	-	88.51	64.38	52.54	58.63	-
	AGLRLS [14]	TMM 2024	61.97	-	87.60	-	-	60.68	-
	DAN [4]	ICML 2015	59.62	59.35	76.46	56.35	51.57	52.72	59.35
	DANN [41]	JMLR 2016	61.03	60.53	77.43	54.23	50.29	54.67	59.67
	ADDA [42]	CVPR 2017	62.91	61.47	80.02	57.50	51.89	53.30	61.18
Source Combine	Source-Only	-	53.52	60.10	77.83	58.44	41.86	42.24	55.67
	DAN [4]	ICML 2015	54.75	62.32	80.34	59.48	47.46	50.52	59.14
	DANN [41]	JMLR 2016	60.56	64.21	79.85	60.78	49.86	51.46	60.95
	ADDA [42]	CVPR 2017	61.50	64.77	83.17	62.86	46.23	51.99	61.75
	AGLRLS [14]	TMM 2024	60.56	65.32	83.80	61.91	49.54	53.27	62.40
Multi-Source	MDAN [29]	NIPS 2018	60.09	63.36	79.29	62.24	48.23	51.16	60.73
	M ³ SDA [44]	ICCV 2019	51.17	65.41	72.57	55.26	46.37	47.62	56.40
	MJD [45]	PR 2024	61.03	68.29	80.48	63.45	49.83	52.43	62.59
	DUML [19]	MM 2023	69.95	73.24	88.57	65.60	52.46	56.56	67.73
	LA-CMFER (ours)	2024	70.42	77.86	90.48	66.50	53.26	57.40	69.32

4 Experiments and Result Analysis

4.1 Experimental Setup

Datasets. To verify the performance of the proposed method, we follow the experiment settings in [19] and involve six commonly used FER datasets, including three lab-controlled datasets CK+ [7], JAFFE [22], and Oulu-CASIA [35] and three Internet-collected large-scale field datasets AffectNet [6], RAF-DB [8], and FER-2013 [21]. Specifically, **CK+** provides 593 annotated video samples from 123 subjects and uses the last three frames with six basic emotions (i.e., anger, disgust, fear, surprise, happy, and sad) and neutral emotions, finally gaining a total of 1,236 images. **JAFFE** includes 213 facial expression images from 10 Japanese women. **Oulu-CASIA (Oulu)** captures 2988 face images by choosing the last three frames with normal lighting for basic expressions and the first frame for neutral expressions. **AffectNet** stands as the largest facial expression dataset to date. Following [19], we curate up to 5,000 facial images for each emotion category, resulting in a total of 33,793 training images and 3,500 testing images. **RAF-DB** is a real-world FER dataset that has 12,271 and 3,068 images for training and testing, respectively. **FER-2013**, compiled via the Google image search engine, contains 35,887 images of different facial expressions and uses 28,709 images for training and 3,589 images for testing. Intuitively, some samples from each dataset are given in Fig. 3.

For label settings, we select the subset with six basic and neutral emotion labels from each dataset, and the training and testing sets of the lab-controlled datasets are the same. In our experiments, each dataset is sequentially regarded as a domain and we utilize the symbol ‘→A’ to represent that dataset A is the target domain while other datasets serve as source domains.

Implementation Details. We conduct all our experiments on two GeForce RTX 3090 GPUs with the PyTorch toolbox. Same as [19], face images are first detected and aligned by the RetinaFace [36] and further resized to 224 × 224. We use the conv1~conv3 layers



Fig. 3. Examples from the six FER datasets.

of ResNet-18 pre-trained on ImageNet [37] as the shared encoder E . The details of the global and local branches are in *Supplementary Materials*. For all datasets, we train the whole framework for 20,000 iterations with a learning rate of 0.01 and a batch size of 128. The setting of the optimizer and learning schedule are kept the same with [38]. In our experiments, we maintain a fixed random seed over 3 runs and report the mean results. The hyper-parameter λ is empirically set as 0.02. For the hyper-parameters in Eq. (14), based on our trial studies, we set α as 0.4 for FER-2013 and AffectNet and 0.1 for the rest. Besides, we set β as 0.5 and γ as 0.1. The reliability threshold ϵ is set as 0.4. To select reliable pseudo labels, τ is set as 0.9 [39, 40]. The code is available at: <https://github.com/YYX-future/LA-CMFER>.

4.2 Comparison Experiments

To verify the effectiveness of the proposed method, we compare our method with state-of-the-art (SOTA) Single-source DA methods (SDA) and MDA methods. For SDA methods, two protocols are adopted: (1) Single Best, which reports the best result among all source domains, and (2) Source Combine, which naively combines all source domains and then uses the SDA methods. Specifically, Source-Only refers to directly transferring the model trained in source domains to the target domain. We select (i) the traditional SDA methods: DAN [4], DANN [41], ADDA [42], and

Table 2: Ablation studies (%) on the contributions of our key components.

Variants	→J	→R	→C	→O	→A	→F	Avg
(A) Baseline	53.52	60.05	84.76	58.40	41.81	42.35	56.82
(B) w. MMD	61.03	73.31	89.05	63.92	50.40	52.94	65.11
(C) w. $H(\cdot)$	66.67	75.88	89.52	63.59	51.03	55.48	67.03
(D) w. \mathcal{L}_{inter}	68.08	76.38	89.04	64.92	51.43	56.28	67.69
(E) w. \mathcal{L}_{mcc}	69.48	77.37	89.71	65.93	52.69	56.84	68.67
(F) w. \mathcal{L}_{mvv}	70.42	77.86	90.48	66.50	53.26	57.40	69.32

Table 3: Comparison results (%) of different inter-domain alignment strategies.

Strategy	→J	→R	→C	→O	→A	→F	Avg
Adv variant	68.54	77.76	89.81	61.85	47.99	52.02	66.33
Ours	70.42	77.86	90.48	66.50	53.26	57.40	69.32

Table 4: Quantitative analysis of features distances achieved by Adv variant, DUML, and our LA-CMFER, respectively.

Methods	Adv variant		DUML		Ours	
	Sources	Target	Sources	Target	Sources	Target
Accuracy (%) \uparrow	-	66.33	-	67.73	-	69.32
(A) Intra-L2 (\downarrow)	0.85	1.40	0.78	1.35	0.69	1.08
(B) Intra-var (\downarrow)	0.02	0.02	0.02	0.02	0.02	0.02
(C) Inter-L2 (\uparrow)	1.32	1.02	1.48	1.06	1.50	1.32
(D) r (\uparrow)	1.55	0.73	1.90	0.78	2.17	1.22

CD-FER method AGLRLS [14] with both protocols. (ii) The CD-FER methods: LGDSTL [13], DMSRL [43], and RANDA [11] are chosen as additional comparison methods for Single Best. For MDA methods, we choose (iii) the typical MDA methods MDAN [29], M^3 SDA [44], and MJD [45]; and (iv) the latest CMFER method DUML [19]. To ensure a fair comparison, the results of these methods are obtained either from their respective papers or by reimplemented using their released code.

The comparison results on different FER datasets are reported in Tab.1 where our LA-CMFER gains the best average accuracy of 69.32% and largely surpasses the second-best DUML by 1.59%. In particular, all Source Combine methods are relatively unpromising, as the inter-domain shifts impair effective knowledge transfer. On the ‘→CK+’ and ‘→FER-2013’ tasks, the SOTA CDFER method AGLRLS experiences considerable performance degradation (i.e., 62.40% average accuracy) when adapting from single-source to multi-source scenarios. This underscores the impracticality of solely relying on the Source Combine strategy to address CMFER tasks. Besides, by tackling the inter-domain shifts, MDA methods gain better performance where MJD obtains 62.59% average accuracy and reaches 68.29% and 63.45% on the ‘→RAF-DB’ and ‘→Oulu’ task, respectively. As a well-designed SOTA CMFER method, DUML achieves the second-best overall performance. Compared to it, our LA-CMFER still keeps its leading accuracy. Especially, on the challenging ‘→RAF-DB’ task, LA-CMFER remarkably surpasses DUML by 4.62%. These experimental results have verified the superior performance of our LA-CMFER.

4.3 Analytical Experiments

Contributions of Key Components: To study the contributions of key components in our LA-CMFER, we progressively conduct ablation experiments on all FER datasets. For clarity, ‘Baseline’ means directly transferring the dual-branch model trained in the source domains to the target domain with only supervised loss \mathcal{L}_{sup} . ‘MMD’ indicates using the traditional MMD loss to assist the network to alleviate the inter-domain shift. The experimental results are shown in Tab.2 where we use the initial letters of the dataset as its reference for the space limitations. As seen, each constraint loss positively contributes to performance enhancements in most cases. With MMD, (B) achieves 8.29% mean promotion by narrowing the inter-domain shift within the dual-branch framework. Compared to (B), the sample-level inter-domain alignment with hardness-aware weighting function $H(\cdot)$, i.e., (C), further enhances the accuracy from 65.11% to 67.03%. Besides, with the additional cluster-level alignment, (D) gains notable promotions on ‘→JAFFE’ (\uparrow 1.41%) and ‘→Oulu’ (\uparrow 1.33%) tasks, respectively. Then, with \mathcal{L}_{mcc} and \mathcal{L}_{mvv} in the multi-view intra-domain alignment, we obtain mean accuracies of 68.67% and 69.32%, respectively.

Impact of Different Inter-domain Alignment Strategies: To explore the impact of different inter-domain alignment strategies, we compare our dual-level inter-domain alignment with the widely used adversarial training strategy [19]. To accomplish adversarial training, rather than employing our dual-level inter-domain alignment, we use two discriminators following our global and local branches to distinguish whether the features come from the source domain or the target domain (denoted as ‘Adv variant’). As seen in Tab.3, our dual-level inter-domain alignment achieves enhancements on all tasks, particularly for the ‘→O’ (\uparrow 4.65%), ‘→A’ (\uparrow 5.27%), and ‘→F’ (\uparrow 5.38%) tasks. These results strongly reveal that, unlike adversarial training, which only aligns multiple domains at a feature level, our method can prioritize hard samples with abundant knowledge and further leverage label information, thus enabling a more fine-grained alignment with higher accuracy.

Further, in the domain alignment, the distances among the data distributions of multiple domains can give a direct evaluation of the alignment effectiveness. Thus, we adopt several distance metrics, involving (A) intra-class L2 distance (intra-L2), (B) intra-class variance (intra-var), (C) inter-class L2 distance (inter-L2), and (D) distance ratio r ($r = \text{inter-L2}/\text{intra-L2}$). The comparisons among the Adv variant, DUML [19], and our LA-CMFER are shown in Tab.4. As seen, compared to both the Adv variant and DUML, our LA-CMFER achieves the least intra-class distances (0.69 for sources and 1.08 for target) and the largest inter-class distances (1.50 for sources and 1.32 for target). Such remarkable superiorities validate that our LA-CMFER can effectively promote inter-class variability and intra-class compactness, thus reaching the best accuracy (69.32%).

Analysis of the Global-Local Branch Architecture: To capture both the global knowledge from the full image and local expression details, LA-CMFER is built with a global-local branch architecture. To study its superiority, we compared five different architectures: (i) only global branch (denoted as ‘Global’), (ii) only local branch

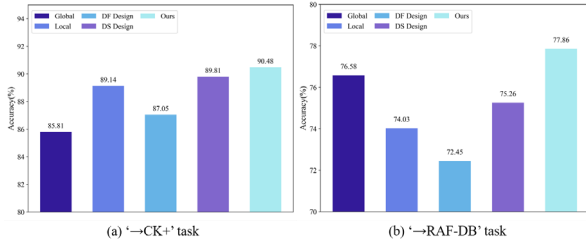


Fig. 4. Experimental results about different global or local architectures on the (a) ‘→CK+’ and (b) ‘→RAF-DB’ tasks.

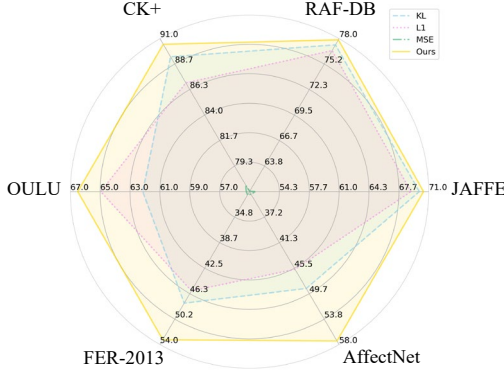


Fig. 5. Experimental results about different cross-view consistency constraints on each task.

Table 6: Analytical experiment of different multi-view pseudo labeling strategies on the ‘→CK+’ and ‘→RAF-DB’ tasks.

Strategy	→CK+	→RAF-DB	Avg
SPL	85.43	74.40	79.92
Ours	90.48	77.86	84.17 (14.25)

(denoted as ‘Local’), (iii) domain-fusion design where the features from the global and local branches are concatenated and fed into a single classifier (denoted as ‘DF Design’), (iv) domain-specific design [19, 30] where a global branch, as well as a local branch, are adopted to each source domain and the final results come from a weighted of all classifiers (denoted as ‘DS Design’), and (v) our global-local branch with only a global classifier and a local classifier. The results are summarized in Fig. 4. DF Design and DS Design sometimes perform worse than Global or Local. This could be due to the distortion of important local and global information, as well as interference from the differences in distribution among multiple sources and their insufficient information interactions. Overall, compared to DS Design, like DUML, our design global-local branch architecture presents a simpler and lighter architecture with no additional discriminators and domain-specific modules, and can better handle the CMFER task adeptly and effectively transfer knowledge across domains.

Impact of Different Cross-view Consistency Constraints: In the intra-domain alignment, the consistency loss enforces the identical predictions of the global and local branches. Here, we explore the performance disparities by using four multi-view consistency constraints in our LA-CMFER network: (i) Kullback-Leibler (KL) divergence, (ii) L1 distance (), (iii) Mean Squared Error (MSE), and

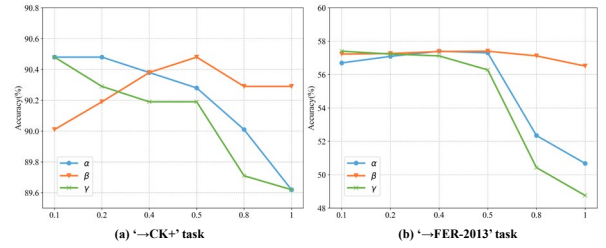


Fig. 6. Experimental results about sensitivity test of hyper-parameters α , β , and γ .

Table 7: Experimental results about different selections of hyper-parameter λ on the ‘→CK+’ and ‘→FER-2013’ tasks.

	Hyper-parameter λ					
	0.01	0.02	0.04	0.06	0.08	0.10
Accuracy (%) on ‘→CK+’	90.19	90.48	90.38	90.29	90.19	89.81
Accuracy (%) on ‘→FER-2013’	57.12	57.40	57.26	57.12	56.78	56.26

(iv) our proposed multi-view clustering consistency loss (\mathcal{L}_{mcc}). Experimental results on each task are displayed in Fig. 5. As seen, KL divergence achieves the second-best accuracies on almost all tasks while our \mathcal{L}_{mcc} surpasses it largely. This verifies that \mathcal{L}_{mcc} better fosters consistency between two branches, thus decreasing the prediction uncertainty and promoting intra-domain alignments. **Impact of the Different Multi-view Pseudo Labeling Strategies:** In the intra-domain alignment, LA-CMFER designs a multi-view voting scheme to provide additional supervision (\mathcal{L}_{mvv}) with the high-quality pseudo labels which are consistently generated by two branches and at least one branch achieves a higher confidence than the threshold τ . Here, we compare our scheme with a separate pseudo labeling (SPL) strategy where each branch is independently constrained with high-confidence pseudo labels within the branch. The experimental results are given in Tab.6. On the ‘→ CK+’ and ‘→RAF-DB’ tasks, our multi-view voting scheme gains 5.05% and 3.46% notable accuracy enhancements, respectively, thus verifying its superiority for global-local knowledge interaction.

Hyper-parameter Sensitivity Tests: In Eq. (14), we utilize hyper-parameters α , β , and γ to balance our four losses. Here, we perform hyper-parameter sensitivity tests to determine the optimal values of the three parameters, and the results are shown in Fig. 6. For the ‘→CK+’ task, when α , β , and γ are respectively set as 0.1, 0.5, and 0.1, we obtain the highest accuracies. And when α , β , and γ are respectively set as 0.4, 0.5, and 0.1, the best results are gained on the ‘→FER-2013’ task. Thus, we set α as 0.4 for the hard dataset FER-2013 and AffectNet while 0.1 for the rest. Besides, we set β and γ as 0.5 and 0.1, respectively. The hyper-parameter λ in Eq. (9) balances the sample- and cluster-level inter-domain alignment, and we try to find its optimal value. Since the cluster-level alignment only finetunes the feature space with label information, we select the value of λ from {0.01, 0.02, 0.04, 0.06, 0.08, 0.10}. As seen in Tab. 7, our model is robust to λ and when λ is set as 0.02, the best accuracies are gained.

Feature visualizations: To assess the transferability of our model, we employ t-SNE visualizations to visualize the feature embeddings of different task models on the ‘→CK+’ task. As illustrated

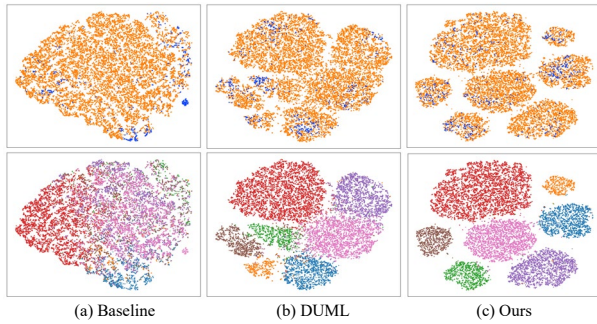


Fig. 7. T-SNE visualizations of feature embeddings on the ‘→CK+’ task. The first row denotes domain information (Orange: source domain; Blue: target domain) while the second row represents category information (Each color denotes a class).

in Fig. 7, the feature embeddings of the Baseline present a noticeable mismatch with the source domain. With domain-uncertainty estimations, DUML better aligns the source domains to the target one but exhibits relatively poor intra-class compactness where the decision boundaries are not clear enough. In contrast, our LA-CMFER surpasses both Baseline and DUML, as evidenced by the formation of clusters with more distinct boundaries. This signifies the superior transferability of our approach which can effectively maintain the strong discrimination capability.

Notably, more additional experiments including ‘Selections of Reliability Threshold ϵ ’, ‘Number of Source Domains’, and so on are given in the Supplementary Materials.

5 Conclusion

In this paper, we present the LA-CMFER framework to achieve the CMFER task by addressing both inter- and intra-domain shifts. We first propose a dual-level (i.e., sample- and cluster-level) inter-domain alignment method to narrow the inter-domain shifts by prioritizing hard-to-align samples and sufficiently using the class attributes. Then, to tackle the intra-domain shifts, a multi-view intra-domain alignment method is introduced to promote consistency between the global and local branches. Extensive experiments have verified the superiority of our LA-CMFER.

6 Acknowledgments

This work is supported by National Natural Science Foundation of China (NSFC 62371325, 62071314), Sichuan Science and Technology Program 2023YFG0263, 2023YFG0025, 2023YFG0101.

REFERENCES

- [1] Yujie Yang, Lin Hu, Chen Zu, Qizheng Zhou, Xi Wu, Jiliu Zhou, and Yan Wang. 2023. Facial Expression Recognition with Contrastive Learning and Uncertainty-Guided Relabeling. *International Journal of Neural Systems* (June 2023). DOI: <https://doi.org/10.1142/s0129065723500326>.
- [2] Kaiming He, Xiangyu Zhang, Shaoqing Ren, and Jian Sun. 2016. Deep Residual Learning for Image Recognition. *In 2016 IEEE Conference on Computer Vision and Pattern Recognition (CVPR)*. DOI: <https://doi.org/10.1109/cvpr.2016.90>
- [3] Gao Huang, Zhuang Liu, Laurens Van Der Maaten, and Kilian Q. Weinberger. 2017. Densely Connected Convolutional Networks. *In 2017 IEEE Conference on Computer Vision and Pattern Recognition (CVPR)*. DOI: <https://doi.org/10.1109/cvpr.2017.243>.

- [4] Mingsheng Long, Yue Cao, Jianmin Wang, and Michael Jordan. 2015. Learning Transferable Features with Deep Adaptation Networks. *arXiv: Learning*, arXiv: Learning (February 2015).
- [5] Boqing Gong, Kristen Grauman, and Fei Sha. 2013. Connecting the Dots with Landmarks: Discriminatively Learning Domain-Invariant Features for Unsupervised Domain Adaptation. *International Conference on Machine Learning, International Conference on Machine Learning* (June 2013).
- [6] Ali Mollahosseini, Behzad Hasani, and Mohammad H. Mahoor. 2019. AffectNet: A Database for Facial Expression, Valence, and Arousal Computing in the Wild. *IEEE Transactions on Affective Computing* (January 2019), 18–31. DOI: <https://doi.org/10.1109/taffc.2017.2740923>.
- [7] Patrick Lucey, Jeffrey F. Cohn, Takeo Kanade, Jason Saragih, Zara Ambadar, and Iain Matthews. 2010. The Extended Cohn-Kanade Dataset (CK+): A complete dataset for action unit and emotion-specified expression. *In 2010 IEEE Computer Society Conference on Computer Vision and Pattern Recognition - Workshops*. DOI: <https://doi.org/10.1109/cvprw.2010.5543262>.
- [8] Shan Li, Weihong Deng, and JunPing Du. 2017. Reliable Crowdsourcing and Deep Locality-Preserving Learning for Expression Recognition in the Wild. *In 2017 IEEE Conference on Computer Vision and Pattern Recognition (CVPR)*. DOI: <https://doi.org/10.1109/cvpr.2017.277>.
- [9] Shan Li and Weihong Deng. 2022. Deep Facial Expression Recognition: A Survey. *IEEE Transactions on Affective Computing* (July 2022), 1195–1215. DOI: <https://doi.org/10.1109/taffc.2020.2981446>.
- [10] I. Michael Revina and W.R. Sam Emmanuel. 2021. A Survey on Human Face Expression Recognition Techniques. *Journal of King Saud University - Computer and Information Sciences* (July 2021), 619–628. DOI: <https://doi.org/10.1016/j.jksuci.2018.09.002>.
- [11] Yanli Ji, Yuhao Hu, Yang Yang, and Heng Tao Shen. 2023. Region Attention Enhanced Unsupervised Cross-Domain Facial Emotion Recognition. *IEEE Transactions on Knowledge and Data Engineering* (April 2023), 4190–4201. DOI: <https://doi.org/10.1109/tkde.2021.3136606>.
- [12] Yanli Ji, Yuhao Hu, Yang Yang, Fumin Shen, and Heng Tao Shen. 2019. Cross-domain facial expression recognition via an intra-category common feature and inter-category Distinction feature fusion network. *Neurocomputing* 333, (March 2019), 231–239. DOI: <https://doi.org/10.1016/j.neucom.2018.12.037>.
- [13] Wenjing Zhang, Peng Song, and Wenming Zheng. 2022. Joint Local-Global Discriminative Subspace Transfer Learning for Facial Expression Recognition. *IEEE Transactions on Affective Computing* (July 2022), 2484 - 2495. DOI: <https://doi.org/10.1109/TAFFC.2022.3168834>.
- [14] Yuefang Gao, Yuhao Xie, ZekeZexi Hu, Tianshui Chen, and Liang Lin. 2024. Adaptive Global-Local Representation Learning and Selection for Cross-Domain Facial Expression Recognition. *IEEE Transactions on Multimedia* (January 2024), 6676 - 6688. DOI: <https://doi.org/10.1109/TMM.2024.3355637>.
- [15] Yuan Xie, Tianshui Chen, Tao Pu, Hefeng Wu, and Liang Lin. 2020. Adversarial Graph Representation Adaptation for Cross-Domain Facial Expression Recognition. *In Proceedings of the 28th ACM International Conference on Multimedia*. DOI: <https://doi.org/10.1145/3394171.3413822>.
- [16] Tianshui Chen, Tao Pu, Hefeng Wu, Yuan Xie, Lingbo Liu, and Liang Lin. 2022. Cross-Domain Facial Expression Recognition: A Unified Evaluation Benchmark and Adversarial Graph Learning. *IEEE Transactions on Pattern Analysis and Machine Intelligence* (December 2022), 9887–9903. DOI: <https://doi.org/10.1109/tpami.2021.3131222>.
- [17] Yingjian Li, Yingnan Gao, Bingzhi Chen, Zheng Zhang, Lei Zhu, and Guangming Lu. 2021. JDMAN: Joint Discriminative and Mutual Adaptation Networks for Cross-Domain Facial Expression Recognition. *In Proceedings of the 29th ACM International Conference on Multimedia*. DOI: <https://doi.org/10.1145/3474085.3475484>.
- [18] Dongliang Chen, Peng Song, and Wenming Zheng. 2023. Learning Transferable Sparse Representations for Cross-Corpus Facial Expression Recognition. *IEEE Transactions on Affective Computing* 14, 2 (April 2023), 1322–1333. DOI: <https://doi.org/10.1109/taffc.2021.3077489>.
- [19] Xuefeng Li, Hanwei Liu, Huiling Cai, and Qingcheng Lin. Learning from More: Combating Uncertainty Cross-multidomain for Facial Expression Recognition. 2023. *In Proceedings of the 31st ACM International Conference on Multimedia*, 5889–5898. DOI: <https://doi.org/10.1145/3581783.3611702>
- [20] Ruihuang Li, Xu Jia, Jianzhong He, Shuaijun Chen, and Qinghua Hu. 2021. T-SVDNet: Exploring High-Order Prototypical Correlations for Multi-Source Domain Adaptation. *In 2021 IEEE/CVF International Conference on Computer Vision (ICCV)*. DOI: <https://doi.org/10.1109/iccv48922.2021.00984>.
- [21] Ian Goodfellow, Dumitru Erhan, Pierre Carrier, Aaron Courville, Mehdi Mirza, Ben Hamner, Will Cukierski, Yichuan Tang, DavidS. Thaler, Dong-Hyun Lee, Yingbo Zhou, Chetan Ramaiah, Fan Feng, Ruifan Li, Xiaojie Wang, Dimitris Athanasakis, John Shawe-Taylor, Maxim Milakov, John Park, Radu Tudor Ionescu, Marius Popescu, Cristian Grozea, James Bergstra, Jingjing Xie, Lukasz Romaszko, Bing Xu, Chuang Zhang, and Yoshua Bengio. 2013. Challenges in Representation Learning: A report on three machine learning contests. *Cornell University - arXiv, Cornell University - arXiv* (July 2013).

- [22] Jihun Hamm, Christian G. Kohler, Ruben C. Gur, and Ragini Verma. 2011. Automated Facial Action Coding System for dynamic analysis of facial expressions in neuropsychiatric disorders. *Journal of Neuroscience Methods* (September 2011), 237–256. DOI: <https://doi.org/10.1016/j.jneumeth.2011.06.023>.
- [23] Garrett Wilson and Diane J. Cook. 2020. A Survey of Unsupervised Deep Domain Adaptation. *ACM Transactions on Intelligent Systems and Technology* (October 2020), 1–46. DOI: <https://doi.org/10.1145/3400066>.
- [24] Tongguang Ni, Cong Zhang, and Xiaoqing Gu. 2021. Transfer Model Collaborating Metric Learning and Dictionary Learning for Cross-Domain Facial Expression Recognition. *IEEE Transactions on Computational Social Systems* 8, 5 (October 2021), 1213–1222. DOI: <https://doi.org/10.1109/tcss.2020.3013938>.
- [25] John Gideon, Melvin G McInnis, and Emily Mower Provost. 2021. Improving Cross-Corpus Speech Emotion Recognition with Adversarial Discriminative Domain Generalization (ADDOG). *IEEE Transactions on Affective Computing* (October 2021), 1055–1068. DOI: <https://doi.org/10.1109/taffc.2019.2916092>.
- [26] Shiliang Sun, Honglei Shi, and Yuanbin Wu. 2015. A survey of multi-source domain adaptation. *Information Fusion* (July 2015), 84–92. DOI: <https://doi.org/10.1016/j.inffus.2014.12.003>.
- [27] Yishay Mansour, Mehryar Mohri, and Afshin Rostamizadeh. 2008. Domain Adaptation with Multiple Sources. *Neural Information Processing Systems, Neural Information Processing Systems* (December 2008).
- [28] John Blitzer, Koby Crammer, Alex Kulesza, Fernando Pereira, and Jennifer Wortman. 2007. Learning Bounds for Domain Adaptation. *Neural Information Processing Systems, Neural Information Processing Systems* (December 2007).
- [29] Han Zhao, Shanghang Zhang, Guanhang Wu, J.M.F. Moura, João Paulo Costeira, and Geoffrey J. Gordon. 2018. Adversarial Multiple Source Domain Adaptation. *Neural Information Processing Systems, Neural Information Processing Systems* (January 2018).
- [30] Yongchun Zhu, Fuzhen Zhuang, and Deqing Wang. 2019. Aligning Domain-Specific Distribution and Classifier for Cross-Domain Classification from Multiple Sources. *Proceedings of the AAAI Conference on Artificial Intelligence* (August 2019), 5989–5996. DOI: <https://doi.org/10.1609/aaai.v33i01.33015989>.
- [31] Yongchun Zhu, Fuzhen Zhuang, Jindong Wang, Guolin Ke, Jingwu Chen, Jiang Bian, Hui Xiong, and Qing He. 2021. Deep Subdomain Adaptation Network for Image Classification. *IEEE Transactions on Neural Networks and Learning Systems* (April 2021), 1713–1722. DOI: <https://doi.org/10.1109/tnnls.2020.2988928>.
- [32] Yiyang Li, Shengsheng Wang, Bilin Wang, Zhiwei Hao, and Hao Chai. 2023. Transferable feature filtration network for multi-source domain adaptation. *Knowledge-Based Systems* 260, (January 2023), 110113. DOI: <https://doi.org/10.1016/j.knsys.2022.110113>.
- [33] Olivier Chapelle, Bernhard Schölkopf, and Jason Weston. 2003. Semi-Supervised Learning through Principal Directions Estimation. *International Conference on Machine Learning, International Conference on Machine Learning* (August 2003).
- [34] Ying Jin, Ximei Wang, Mingsheng Long, and Jianmin Wang. 2020. Minimum Class Confusion for Versatile Domain Adaptation. In *Computer Vision – ECCV 2020, Lecture Notes in Computer Science*. 464–480. DOI: https://doi.org/10.1007/978-3-030-58589-1_28.
- [35] Guoying Zhao, Xiaohua Huang, Matti Taini, Stan Z. Li, and Matti Pietikäinen. 2011. Facial expression recognition from near-infrared videos. *Image and Vision Computing* (August 2011), 607–619. DOI: <https://doi.org/10.1016/j.imavis.2011.07.002>.
- [36] Jiankang Deng, Jia Guo, Evangelos Ververas, Irene Kotsia, and Stefanos Zafeiriou. 2020. RetinaFace: Single-Shot Multi-Level Face Localisation in the Wild. In *2020 IEEE/CVF Conference on Computer Vision and Pattern Recognition (CVPR)*. DOI: <https://doi.org/10.1109/cvpr42600.2020.00525>.
- [37] Jia Deng, Wei Dong, Richard Socher, Li-Jia Li, Kai Li, and Li Fei-Fei. 2009. ImageNet: A large-scale hierarchical image database. In *2009 IEEE Conference on Computer Vision and Pattern Recognition*. DOI: <https://doi.org/10.1109/cvpr.2009.5206848>.
- [38] Yueming Yin, Zhen Yang, Haifeng Hu, and Xiaofu Wu. 2022. Universal multi-source domain adaptation for image classification. *Pattern Recognition* (January 2022), 108238. DOI: <https://doi.org/10.1016/j.patcog.2021.108238>.
- [39] Kuniaki Saito, Yoshitaka Ushiku, and Tatsuya Harada. 2017. Asymmetric Tri-training for Unsupervised Domain Adaptation. *arXiv: Computer Vision and Pattern Recognition, arXiv: Computer Vision and Pattern Recognition* (February 2017).
- [40] Ruijia Xu, Ziliang Chen, Wangmeng Zuo, Junjie Yan, and Lin Li. 2018. Deep Cocktail Network: Multi-source Unsupervised Domain Adaptation with Category Shift. *Proceedings of the IEEE conference on computer vision and pattern recognition*, 3964–3973.
- [41] Ganin Yaroslav, Ganin Yaroslav, Ustinova Evgeniya, Ustinova Evgeniya, Ajakan Hana, Germain Pascal, Germain Pascal, Larochelle Hugo, Larochelle Hugo, Laviolette François, Laviolette François, Marchand Mario, Marchand Mario, and Lempitsky Victor, Lempitsky Victor. 2016. Domain-adversarial training of neural networks. *Journal of Machine Learning Research*, (January 2016).
- [42] Eric Tzeng, Judy Hoffman, Kate Saenko, and Trevor Darrell. 2017. Adversarial Discriminative Domain Adaptation. In *2017 IEEE Conference on Computer Vision and Pattern Recognition (CVPR)*. DOI: <https://doi.org/10.1109/cvpr.2017.316>.
- [43] Yingjian Li, Zheng Zhang, Bingzhi Chen, Guangming Lu, and David Zhang. 2023. Deep Margin-Sensitive Representation Learning for Cross-Domain Facial Expression Recognition. *IEEE Transactions on Multimedia* (January 2023), 1359–1373. DOI: <https://doi.org/10.1109/tmm.2022.3141604>.
- [44] Xingchao Peng, Qinxun Bai, Xide Xia, Zijun Huang, Kate Saenko, and Bo Wang. 2019. Moment Matching for Multi-Source Domain Adaptation. In *2019 IEEE/CVF International Conference on Computer Vision (ICCV)*. DOI: <https://doi.org/10.1109/iccv.2019.00149>.
- [45] Sentao Chen. 2024. Multi-Source Domain Adaptation with Mixture of Joint Distributions. *Pattern Recognition*, 2024, 149: 110295. DOI: <https://doi.org/10.1016/j.patcog.2024.110295>.
- [46] Lijuan Wang, Guoli Jia, Ning Jiang, Haiying Wu, and Jufeng Yang. 2022. EASE: Robust Facial Expression Recognition via Emotion Ambiguity-SEnsitive Cooperative Networks. In *Proceedings of the 30th ACM International Conference on Multimedia*. DOI: <https://doi.org/10.1145/3503161.3548005>.
- [47] Zengqun Zhao and Qingshan Liu. 2021. Former-DFER: Dynamic Facial Expression Recognition Transformer. In *Proceedings of the 29th ACM International Conference on Multimedia*. DOI: <https://doi.org/10.1145/3474085.3475292>.
- [48] Yi Wu, Shangfei Wang, and Yanan Chang, Y. 2023. Patch-Aware Representation Learning for Facial Expression Recognition. In *Proceedings of the 31st ACM International Conference on Multimedia*. (2023, October), 6143–6151. DOI: <https://doi.org/10.1145/3581783.3612342>.
- [49] Jianjian Shao, Zhenqian Wu, Yuanyan Luo, Shudong Huang, Xiaorong Pu, and Yazhou Ren. 2022. Self-Paced Label Distribution Learning for In-The-Wild Facial Expression Recognition. In *Proceedings of the 30th ACM International Conference on Multimedia*. (October 2022), 161–169. DOI: <https://doi.org/10.1145/3503161.3547960>.
- [50] Zengmao Wang, Chaoyang Zhou, Bo Du, and Fengxiang He. 2022. Self-paced Supervision for Multi-Source Domain Adaptation. *International Joint Conference on Artificial Intelligence* (July 2022).
- [51] Kaiyang Zhou, Yongxin Yang, Yu Qiao, and Tao Xiang. 2021. Domain Adaptive Ensemble Learning. *IEEE Transactions on Image Processing* (January 2021), 8008–8018. DOI: <https://doi.org/10.1109/tip.2021.3112012>.
- [52] Muhammad Osama Zeeshan, Muhammad Haseeb Aslam, Soufiane Belharbi, Alessandro L. Koerich, Marco Pedersoli, Simon Bacon, and Eric Granger. 2023. Subject-Based Domain Adaptation for Facial Expression Recognition. (December 2023).

Supplementary Materials

Learning with Alignments: Tackling the Inter- and Intra-domain Shifts for Cross-multidomain Facial Expression Recognition

• Implementation Details of The Global and Local Branches

The global branch consists of a series of convolutional layers and Convolutional Block Attention Modules (CBAMs) [1], while the local branch only consists of a series of convolutional layers. Concretely, the global module expands the dimension of the features from 128 to 1024 after the shared encoder; the local module crops the features from the shared encoder into four regions, and expands the dimensions of these regions from 128 to 256, finally merging them. The final model codes and algorithm codes will be released publicly once the paper is accepted.

• Impact of Selections of Reliability Threshold ϵ

In our inter-domain alignment, we select only those samples with probabilities exceeding the reliability threshold ϵ which balances the positive knowledge transfer and the number of aligned samples. We conduct the threshold selection experiments on the ‘ \rightarrow CK+’ and ‘ \rightarrow FER-2013’ tasks and the results are tabulated in Tab.S.1. As seen, our LA-CMFER achieves a relatively robust performance under different reliability thresholds and when ϵ is set as 0.4, the best accuracies on the two tasks are obtained. Therefore, we set ϵ as 0.4 in all our experiments.

Table S.1: Experimental results about different selections of reliability threshold ϵ on the ‘ \rightarrow CK+’ and ‘ \rightarrow FER-2013’ tasks.

	Threshold ϵ			
	0.0	0.2	0.4	0.6
Accuracy (%) on ‘ \rightarrow CK+’	89.71	90.19	90.48	90.29
Accuracy (%) on ‘ \rightarrow FER-2013’	56.78	57.26	57.40	56.84

• Impact of the Number of Source Domains

We also study how the number of source domains impacts the performance. Here, we progressively add the number of source domains on the ‘ \rightarrow CK+’ and ‘ \rightarrow RAF-DB’ tasks, and the classification accuracies are displayed in Tab. S.2. As observed, as the number of source domains increases, the domain shifts become increasingly complex. Even under such challenging circumstances, our proposed LA-CMFER can effectively align the data distributions among several sources and deeply mine their

Table. S.2: Analytical experiment of impacts on different number of source domains.

Tasks	Accuracy (%)	Tasks	Accuracy (%)
A \rightarrow C	81.71	A \rightarrow R	70.27
A, R \rightarrow C	86.10	A, J \rightarrow R	71.00
A, R, J \rightarrow C	86.48	A, J, F \rightarrow R	74.86
A, R, J, F \rightarrow C	88.00	A, J, F, O \rightarrow R	75.72
A, R, J, F, O \rightarrow C	90.48	A, J, F, O, C \rightarrow R	77.86

beneficial expression features, thus finally gaining gradually enhanced accuracies on both ‘ \rightarrow CK+’ and ‘ \rightarrow RAF-DB’ tasks.

• Quantitative Analysis of Different Cross-view Consistency Constraints

To intuitively evaluate the effectiveness of different cross-view consistency Constraints, we give the quantitative results of different cross-view consistency constraints in Table.S.3. As depicted in Table.S.3, the model’s performance declines to varying degrees when using these alternative strategies instead of our \mathcal{L}_{mcc} . Concretely, while KL and L1 exhibit comparable performance in simple ‘ \rightarrow C’ and ‘ \rightarrow R’ tasks, they show significant performance deterioration in more complex tasks like ‘ \rightarrow A’ and ‘ \rightarrow F’ tasks. This underscores the unreliability of solely considering absolute prediction distances or differences in relative entropy to address intra-domain shifts across FER domains. Additionally, due to substantial intra-domain shifts, the global and local branches may exhibit significant prediction biases for challenging samples near decision boundaries, leading to notable performance fluctuations with the MSE loss which is more sensitive to outliers. In summary, with our multi-view clustering technique, our model can better foster consistency between two branches, thus decreasing the prediction uncertainty and promoting intra-domain alignments.

• Analysis of Hyper-parameter Sensitivity Tests

We conduct further analysis for hyperparameters sensitivity tests of

Table S.3: Quantitative results (%) of different cross-view consistency constraints.

Variants	\rightarrow J	\rightarrow R	\rightarrow C	\rightarrow O	\rightarrow A	\rightarrow F	Avg
(A) KL	69.95	77.30	89.33	62.15	47.76	48.82	65.89
(B) L1	69.01	76.67	86.95	64.96	45.91	45.70	64.87
(C) MSE	51.64	61.04	77.62	55.22	31.50	33.44	51.74
(D) \mathcal{L}_{mcc} (Ours)	70.42	77.86	90.48	66.50	53.26	57.40	69.32

α , β , and γ . Concretely, the three hyperparameters control the importance of the dual-level inter-domain alignment, the cross-view consistency constraint, and the multi-view voting loss, respectively. We select candidate values for α , β , γ from the set $\{0.1, 0.2, 0.4, 0.5, 0.8, 1\}$ and conduct hyperparameters sensitivity tests on the relatively simple ‘ \rightarrow CK+’ task and the more challenging ‘ \rightarrow FER-2013’ task. Based on the observations from Fig. 6 in the manuscript, we summarize our findings as follows: (1) The model exhibits robustness to all hyperparameters in the ‘ \rightarrow CK+’ task, while performance shows a decreasing trend with larger values of α and γ in the more complex ‘ \rightarrow FER-2013’ task; (2) In complex ‘ \rightarrow FER-2013’ task which exits more severe inter-domain shifts, excessively large inter-domain alignment hyperparameter settings may lead the model to over-align on erroneous source-

target domain features and learn misleading ‘discriminative’ features inevitably that may damage the model’s discriminative ability; (3) For the challenging ‘ \rightarrow FER-2013’ task, excessive reliance on supervision for unlabeled target samples may lead to learning from noisy labels, thus degrading performance; (4) Finally, to optimize performance, we set α as 0.4 for the hard dataset FER-2013 and AffectNet while 0.1 for the rest. Meanwhile, we set β and γ as 0.5 and 0.1, respectively.

● **Complexity Analysis**

We compare the computational and time complexity between the proposed and DUML. As shown in Table.S.4, with domain-specific network and discriminators, DUML exhibits 56.85M model Params and 9.36G MACs. In contrast, our method is built on a shared global-local branch without discriminators and shows a reduction of 28.77M Params, 5.16G MACs, and 4.96h training time.

Table.S.4 Complexity comparison between DUML and Ours.

Methods	Params (M)	MACs (G)	Training Time (h)	Inference Time (s)
DUML	56.85	9.36	13.18	3.84
Ours	28.08	4.20	8.22	3.59

REFERENCES

[1] Sanghyun Woo, Jongchan Park, Joon-Young Lee, and In So Kweon. 2018. CBAM: Convolutional Block Attention Module. In Computer Vision – ECCV 2018, Lecture Notes in Computer Science. 3–19. DOI:https://doi.org/10.1007/978-3-030-01234-2_1.